

# Selective Anodic Dissolution of Ag–Zn Alloys in the Eutectic Melt of Alkali Metal Chlorides at 300°C

N. P. Kulik<sup>a,\*</sup>, N. I. Shurov<sup>a</sup>, and N. K. Tkachev<sup>a,\*\*</sup>

<sup>a</sup> Institute of High-Temperature Electrochemistry, Ural Branch, Russian Academy of Sciences, Yekaterinburg, Russia

\*e-mail: n.p.kulik@gmail.com

\*\*e-mail: n.k.tkachev@gmail.com

Received November 3, 2020; revised November 3, 2020; accepted November 20, 2020

**Abstract**—The peculiarities of electrochemical dealloying of two homogeneous Ag–Zn alloys in the  $(\text{LiCl})_{0.57}(\text{CsCl})_{0.26}(\text{KCl})_{0.17}$  melt are studied. The zinc content in the alloys is 67 and 46 mol % which corresponds to the  $\epsilon$  and  $\beta$  phases in the phase diagram at 300°C. Polarization curves are measured and the corrosion potential is determined to be  $-0.78$  and  $-0.55$  V, respectively, vs. Ag/AgCl reference electrode. The complete removal of zinc from the alloy surface is achieved by dealloying in the galvanostatic mode at the current density of about 20 mA/cm<sup>2</sup> for the  $\epsilon$  phase and 7 mA/cm<sup>2</sup> for the  $\beta$  phase. On the surface of the  $\text{Zn}_{0.67}\text{Ag}_{0.33}$  alloy, the characteristic homogeneous porous structures are formed in which the pores and the ligaments are approximately of the same size in the interval of 0.5–5  $\mu\text{m}$ . For the  $\text{Zn}_{0.46}\text{Ag}_{0.54}$  alloy, the dendrite structures with the silver particle size of about 0.5–4 and 5–20  $\mu\text{m}$  are obtained.

**Keywords:** dealloying, molten salts, porous silver

**DOI:** 10.1134/S1023193521050086

## INTRODUCTION

The literature contains a large number of publications summarized in several reviews [1, 2], which are devoted to synthesizing nano and microporous metals including silver by electrochemical dealloying, i.e., selective anodic dissolution of alloys in aqueous media. The interest in nanoporous silver is associated with the possibility of using it as a selective catalyst for hydrogenation of unsaturated hydrocarbons [3], electrochemical reduction of carbon dioxide [4], and electrochemical oxidation of aldehydes [5]. Such silver can serve as the anode in fuel cells [6–8] working on ethanol, ethylene glycol, and borazane and also is promising as the substrate for surface-enhanced Raman spectroscopy [9]. Exhibiting the catalytic effect only a little weaker as compared with gold and platinum-group metals, the much cheaper nanoporous silver can serve as their alternative in redox processes [10, 11]. The antibacterial properties of this material are important for challenging medicinal applications, and its sensitivity with respect to UV radiation is significant for electrical and photo engineering.

To date, the conditions and certain main mechanisms of the percolation dealloying in aqueous solutions, i.e., the selective dissolution of alloys to form bicontinuous systems of pores and ligaments, are already well known. As a rule, the active component content in the alloy should be about 40–60 mol %, and the potential applied or the current passed should

provide the electrolysis conditions such that the rate of removal of electroactive metal ions to the electrolyte bulk exceeds the diffusion rate of the more noble metal on the surface of the remaining metal phase [2, 12, 13]. For silver alloys, the active components are most often zinc [14–19] and aluminum [20, 21]; the more complex compositions are also used, e.g., Ce–Cu–Ag [22] and Y–Mg–Ag [23]. As the electrolyte, the aqueous solutions of acids are used: sulfuric [14–17], hydrochloric [18], or nitric [16]; the neutral solutions are used more rarely [18]. The authors of [23] carried out the selective dissolution of Y–Mg–M alloys (M = Ni, Cu, Pd, Ag, Au) in aqueous solutions of organic acids which served not only as oxidants but also as the surface-active substances which impeded the surface diffusion of metals.

The scarce studies of dealloying in low-temperature ionic liquids [24] have only half-revealed the possibilities of using nonaqueous media stable at high temperatures. Their advantages as compared with aqueous media may include the intensification of the process, the absence of sources of hydrogen and oxygen *in status nascendi*, and the possibility of exerting control over the formation of porous structures by choosing the appropriate temperature mode.

The main idea of this study is to use molten salts as the electrolyte in solving the problems associated with specific features of high-temperature dealloying. Recently, we have made the first steps toward studying

this type of specific anodic dissolution for Al–Au and Cu–Au alloys and also high-grade brass in chloride and carbonate melts [25, 26]. We have found that dealloying of these alloys in molten salt mixtures proceeds faster as compared with their dealloying in aqueous solutions and can produce a microporous structure (with the pore size from 0.1 to several tens  $\mu\text{m}$ ). It is quite evident that the nature of alloy and the temperature can affect the pore size. However, the important questions on the effect of the phase composition of original alloys and the electrolysis parameters on the porous metal morphology are still open.

As the dealloying objects, we have chosen two homogeneous Zn–Ag alloys with the  $\text{Zn}_{0.67}\text{Ag}_{0.33}$  and  $\text{Zn}_{0.46}\text{Ag}_{0.54}$  composition; as the electrolyte, we used the  $(\text{LiCl})_{0.57}(\text{CsCl})_{0.26}(\text{KCl})_{0.17}$  eutectics with the melting point at  $260^\circ\text{C}$ . The difference between the standard electrode potentials of Zn and Ag in chloride melts calculated based on thermodynamic data [27] is 0.74 V at  $300^\circ\text{C}$ . This value is sufficiently high to allow the possibility of selective dissolution of zinc from the alloy. The concrete goal of this study was to investigate how the conditions of electrochemical dealloying in percolation mode affect the shape and size of pores in surface layers of these alloys.

## EXPERIMENTAL

Ag–Zn alloys were obtained by dissolving pieces of silver wire (99.9 wt %) in molten zinc (analytical grade) in a quartz tube in argon atmosphere under  $(\text{LiCl})_{0.57}(\text{CsCl})_{0.26}(\text{KCl})_{0.17}$  flux at  $680^\circ\text{C}$ . After homogenization, the metal was drawn into a quartz tube with the inner diameter of 3 mm. The thus prepared rods were cut to obtain cylinders with the height of 25–30 mm. An end of such cylinder was polished to mirror brightness on metallographic complex Struers (Struers ApS, Denmark). The alloys were tested by means of XRD device Rigaku D/MAX-2200VL/PC (Rigaku, Japan) and emission spectrometer with inductively coupled plasma Optima 4300 DV (Perkin Elmer, USA).

The electrolyte was prepared from salts (reagent grade). Sodium chloride was dried by freezing out moisture at the liquid nitrogen temperature, chlorinated, and subjected to three-fold zone melting to remove oxygen-containing impurities. The further manipulations with lithium chloride were carried out in a dry box. Potassium and cesium chlorides were melted in air. Approximately 50 g of salts in the required ratios were molten in inert atmosphere and homogenized at  $800^\circ\text{C}$  before each experiment.

The measurements were carried out in a three-electrode cell (Fig. 1) in atmosphere of dry purified argon. The melt was placed in SU-1200 glassy-carbon crucible, which also served as the counter electrode for polarization. The Ag/AgCl reference electrode, i.e.,  $\text{Ag}[(\text{LiCl})_{0.57}(\text{CsCl})_{0.26}(\text{KCl})_{0.17}]$  eutectics + 3 mol %

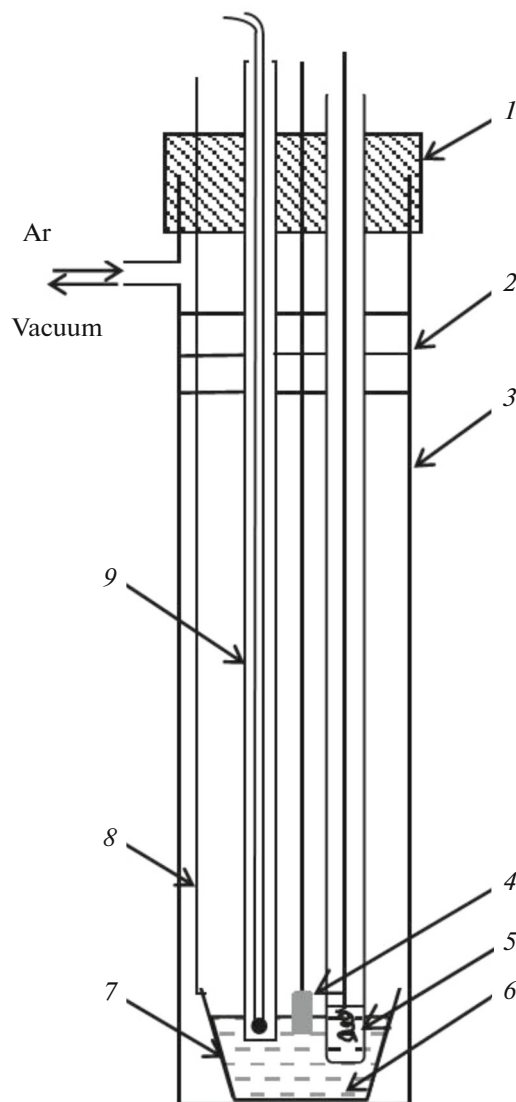


**Fig. 1.** Cell for electrochemical measurements: (1) rubber stopper, (2) heat-reflecting screens (3) quartz tube, (4) Ag–Zn alloy, (5) Ag/AgCl reference electrode in alumina crucible (6) salt melt, (7) glassy carbon crucible, (8) current terminal (Mo), (9) thermocouple.

AgCl, was placed into an alumina crucible with orifices in its walls to provide contact with the working electrolyte. Below, all the potential values are referred to this electrode.

At the temperature of  $300^\circ\text{C}$ , the working electrode was immersed into the melt to the depth of 2–8 mm; after this the measurements were carried out by means of Autolab 302N system (Metrohm, Switzerland). The dealloying was carried out in the potentiostatic and galvanostatic modes by varying either the applied potential or the current and also the electrolysis time. At the end of each experiment, the electrode was washed from salt by distilled water and ethanol, and then the surface of the electrode/melt boundary was assessed visually. The effective current density was cal-

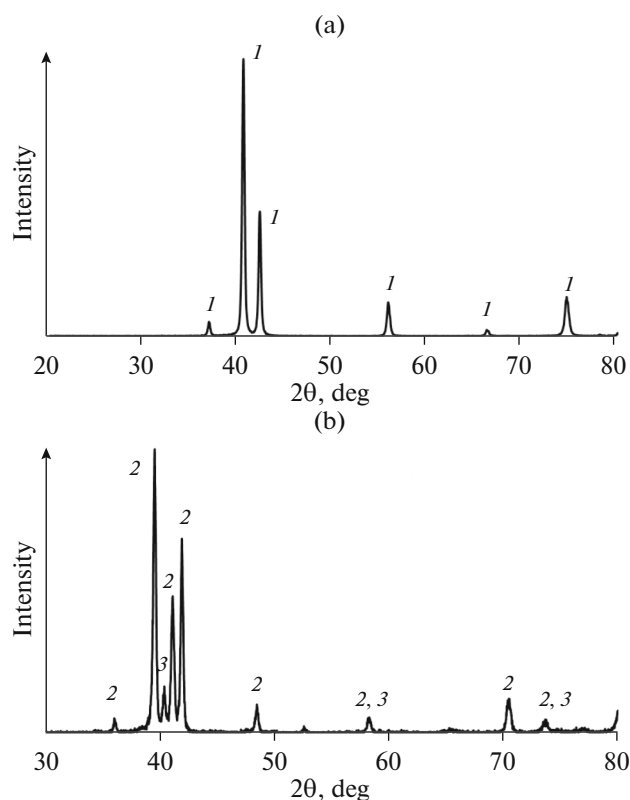


**Fig. 2.** Diffraction patterns of alloys (a)  $\text{Zn}_{0.67}\text{Ag}_{0.33}$  and (b)  $\text{Zn}_{0.46}\text{Ag}_{0.54}$ : spectrum lines of phases (1)  $\epsilon$ , (2)  $\zeta$ , and (3)  $\beta'$ .

culated by the formula  $i = I/S_{\text{geom}}$ , where  $I$  is the current,  $S_{\text{geom}}$  is the geometrical surface of the electrode/melt interface. The X-ray microanalysis of the electrode's end surface was carried out on electron microscopes JSM-5900LV (Jeol, Japan) and TESCAN MIRA 3 LMU (TESCAN, Czech Republic).

## RESULTS AND DISCUSSION

According to the results of elemental chemical analysis, the synthesized alloys had the  $\text{Zn}_{0.67}\text{Ag}_{0.33}$  and  $\text{Zn}_{0.46}\text{Ag}_{0.54}$  composition. Figure 2 shows the results of XRD analysis. In the diffraction pattern of  $\text{Zn}_{0.67}\text{Ag}_{0.33}$  alloy, all the peaks coincide with the lines of the spectrum of the  $\epsilon$ -phase in the Ag–Zn system (PDF#25-1325). The peaks in diffraction pattern of the  $\text{Zn}_{0.46}\text{Ag}_{0.54}$  alloy correspond to the hexagonal  $\zeta$  phase and the unstable cubic  $\beta$  phase (PDF#29-1156 and PDF#29-1155, respectively). At the temperature above  $274^\circ\text{C}$ , these both modifications are transformed to the  $\beta$  phase [28].

Figures 3 and 4 show the anodic voltammetric curves for samples of these alloys and also for pure metals, measured at the potential scan rate of  $1\text{ mV/s}$ . As the anodic potential of the  $\text{Zn}_{0.67}\text{Ag}_{0.33}$  increases

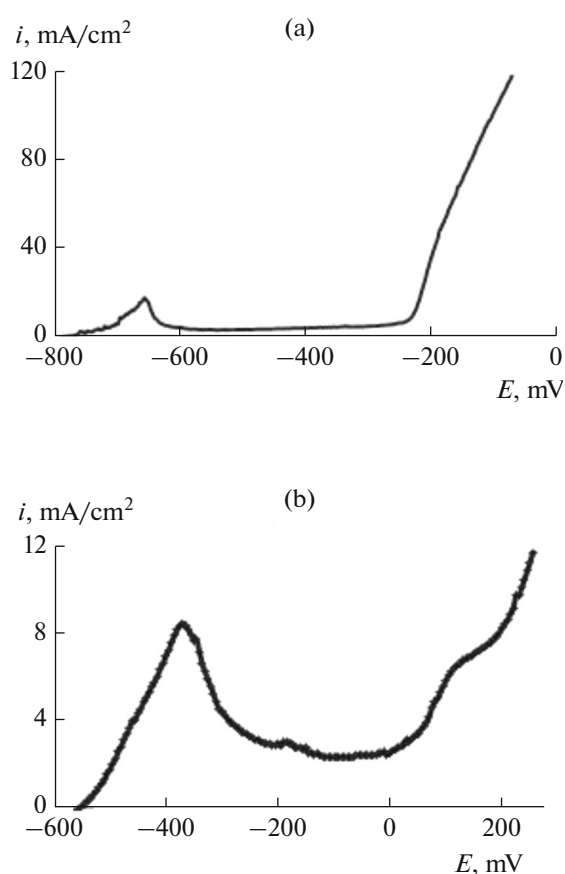


**Fig. 3.** Anodic voltammetric curves of alloys (a)  $\text{Zn}_{0.67}\text{Ag}_{0.33}$  and (b)  $\text{Zn}_{0.46}\text{Ag}_{0.54}$  in  $(\text{LiCl})_{0.57}(\text{CsCl})_{0.26}(\text{KCl})_{0.17}$  melt at  $300^\circ\text{C}$ .

(Fig. 3a), the current density also increases and reaches the maximum at about  $-0.67\text{ V}$  after which decreases almost 4-fold. This is apparently explained by depletion of the metal surface with zinc and also by diffusion limitations for zinc delivery from the metal bulk. The  $i(E)$  dependence of the sample has a plateau in the potential region from  $-0.6\text{ V}$  up to the silver dissolution potential (about  $-0.25\text{ V}$ ).

In the voltammetric curve of  $\text{Zn}_{0.46}\text{Ag}_{0.54}$  alloy (Fig. 3b), the zinc dissolution peak is shifted by  $0.3\text{ V}$  in the anodic direction and the current density in the maximum is lower as compared with the  $\text{Zn}_{0.67}\text{Ag}_{0.33}$  sample. The silver dissolution begins in the vicinity of  $1\text{ V}$ .

Figure 5 shows the corrosion potentials  $E_{\text{cor}}$  calculated for all these samples based on cyclic voltammetric curves.

The potential at which the current density is equal to  $1\text{ mA/cm}^2$  is usually considered as the critical dealloying potential  $E_{\text{cr}}$  [29]. Table 1 shows the values  $E_{\text{cor}}$  and  $E_{\text{cr}}$ .

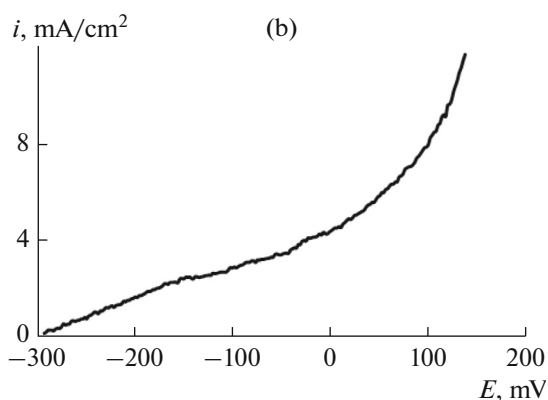
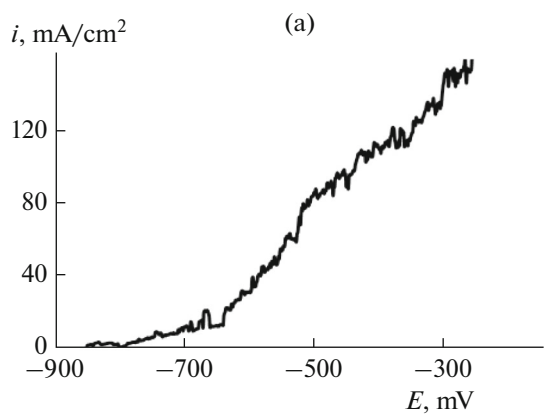


**Fig. 4.** Anodic voltammetric curves of (a) Zn and (b) Ag in  $(\text{LiCl})_{0.57}(\text{CsCl})_{0.26}(\text{KCl})_{0.17}$  melt at  $300^\circ\text{C}$ .

Under potentiostatic conditions, the electrolysis was carried out at the potential by 100–400 mV more positive than the critical dealloying potential. Figure 6 shows typical chronoamperograms of these alloys: the  $\text{Zn}_{0.67}\text{Ag}_{0.33}$  sample is dissolved at the potential of  $-0.60$  V (0.17 V more positive than the critical dealloying potential of this alloy), the  $\text{Zn}_{0.46}\text{Ag}_{0.54}$  sample is dissolved at  $-0.18$  V (0.34 V more positive than  $E_{\text{cr}}$ ). In both cases, the current density decreases by an order of

**Table 1.** Corrosion potentials and critical potentials of dealloying

Sample	Temperature, $^\circ\text{C}$	$E$ , V	
		corrosion potential	critical dealloying potential
$\text{Zn}_{0.67}\text{Ag}_{0.33}$	300	$-0.79$	$-0.77$
$\text{Zn}_{0.46}\text{Ag}_{0.54}$	300	$-0.55$	$-0.52$
Ag	300	$-0.29$	
Zn	300	$-0.86$	

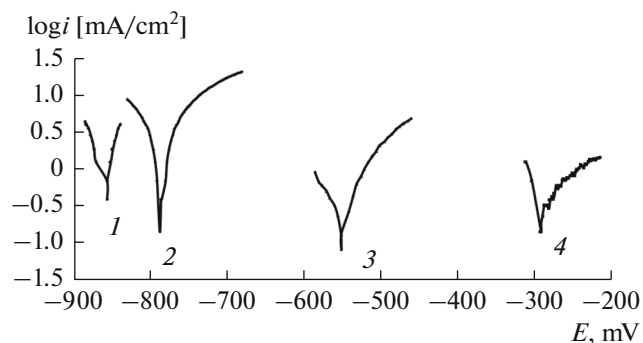


**Fig. 5.** Corrosion potentials of (1) Zn, (2)  $\text{Zn}_{0.67}\text{Ag}_{0.33}$ , (3)  $\text{Zn}_{0.46}\text{Ag}_{0.54}$ , and (4), Ag in  $(\text{LiCl})_{0.57}(\text{CsCl})_{0.26}(\text{KCl})_{0.17}$  melt at  $300^\circ\text{C}$ .

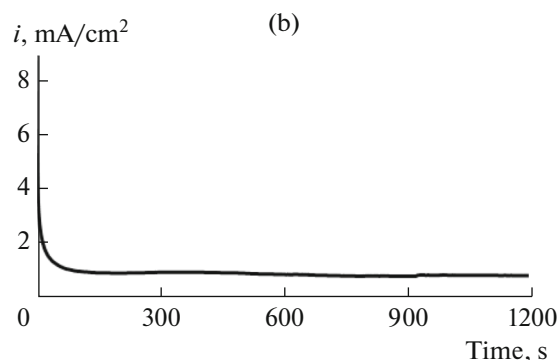
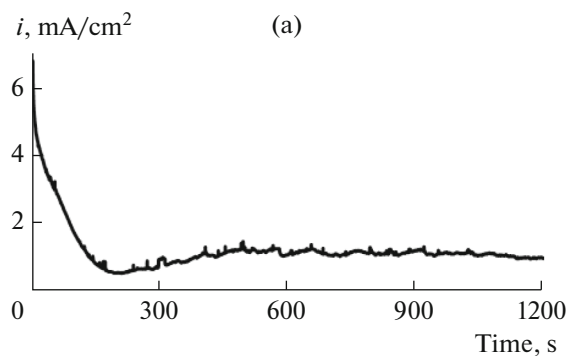


**Fig. 6.** Chronoamperograms of alloys in  $(\text{LiCl})_{0.57}(\text{CsCl})_{0.26}(\text{KCl})_{0.17}$  melt at  $300^\circ\text{C}$ : (a)  $\text{Zn}_{0.67}\text{Ag}_{0.33}$ ,  $E = -600$  mV; (b)  $\text{Zn}_{0.46}\text{Ag}_{0.54}$ ,  $E = -170$  mV.

magnitude in the first minutes, which is associated with active formation of pores.

Figure 7 shows microimages of samples after 30 min dealloying which allowed the initial stage of pore formation to be observed. To that moment, the surface composition of two alloys turned out to be substantially different: the zinc content in the  $\text{Zn}_{0.67}\text{Ag}_{0.33}$  sample decreased by merely several percent, whereas the surface of  $\text{Zn}_{0.46}\text{Ag}_{0.54}$  alloy contained no more than 1–3 mol % Zn. The reason for this, besides the

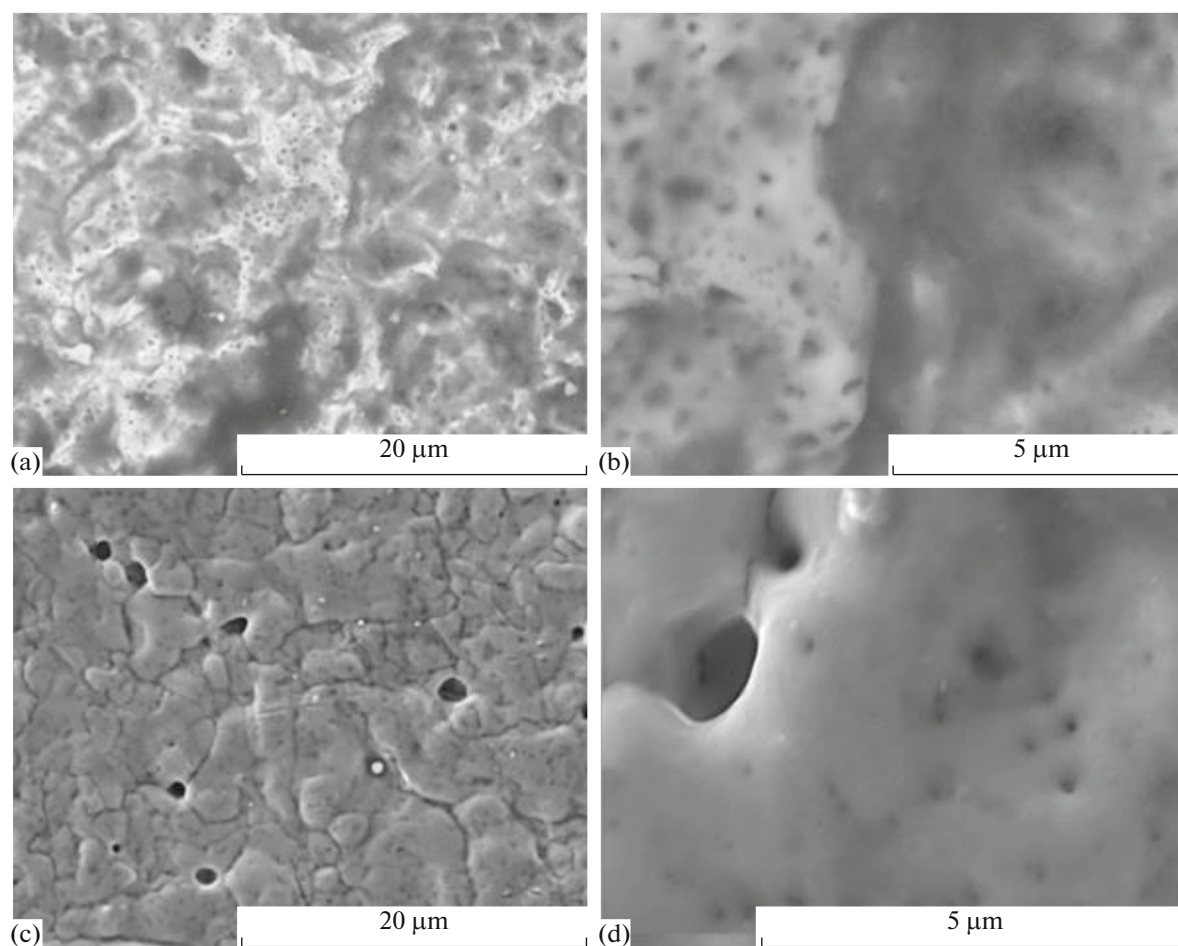


**Fig. 7.** Microimages of the alloy surface after dealloying for 1800 s: (a, b)  $\text{Zn}_{0.67}\text{Ag}_{0.33}$ ,  $E = -600$  mV; (c, d)  $\text{Zn}_{0.46}\text{Ag}_{0.54}$ ,  $E = -170$  mV.

more noble initial composition, may be the fact that the electrolysis in this case occurred at the potential much more positive than the critical dealloying potential.

In the galvanostatic mode, the current density was in the interval of 20–50 mA/cm<sup>2</sup>. Figure 8 shows chronopotentiograms of alloys under study. When the current of the density of 20 and 35 mA/cm<sup>2</sup> flowed (Figs. 8a and 8b) through the  $\text{Zn}_{0.67}\text{Ag}_{0.33}$  alloy, the potential of about  $-0.06$  V was established, which corresponded to the silver surface. The increase in the current density to 50 mA/cm<sup>2</sup> (Fig. 8c) shifted the surface potential in the negative direction in the initial moment. This effect can probably be associated with the fast formation of deep pores and (or) the dissolution of silver together with zinc. After this, the surface proceeded to acquire the more positive potential.

During the galvanostatic electrolysis of the  $\text{Zn}_{0.46}\text{Ag}_{0.54}$  alloy, even at a small current density of 7 mA/cm<sup>2</sup>, the metal surface acquired very quickly the high positive potential (Fig. 8d), i.e., became the “silver” surface.

Figure 9 shows the surface microimages of the  $\text{Zn}_{0.67}\text{Ag}_{0.33}$  alloy after galvanostatic electrolysis. Dealloying with the current density of 35 mA/cm<sup>2</sup> for 1800 s (Figs. 9e and 9f) led to the formation of porous structures with pores and ligaments of the comparable size in the interval from 0.5 to several μm. The residual content of zinc was about 10 mol %. The increase in the electrolysis time at the slightly lower current density of 20 mA/cm<sup>2</sup> (Figs. 9a–9d) made the surface more lacy due to the decrease in the size of ligaments, while the pore diameter remained unchanged. In this case, the surface layer was virtually 100% silver. The similar structures were obtained also when the current of 50 mA/cm<sup>2</sup> was passed for 1800 s (Figs. 9g, 9h); however, they contained a large amount of residual zinc, up to 20 mol %.

Figure 10 shows the microimages of the surface of  $\text{Zn}_{0.46}\text{Ag}_{0.54}$  alloy after galvanostatic electrolysis.

The dealloying at the current density of 7 mA/cm<sup>2</sup> for 3600 s led to formation of the hierarchical structure formed by ligaments measuring from 0.5 to 2 μm and

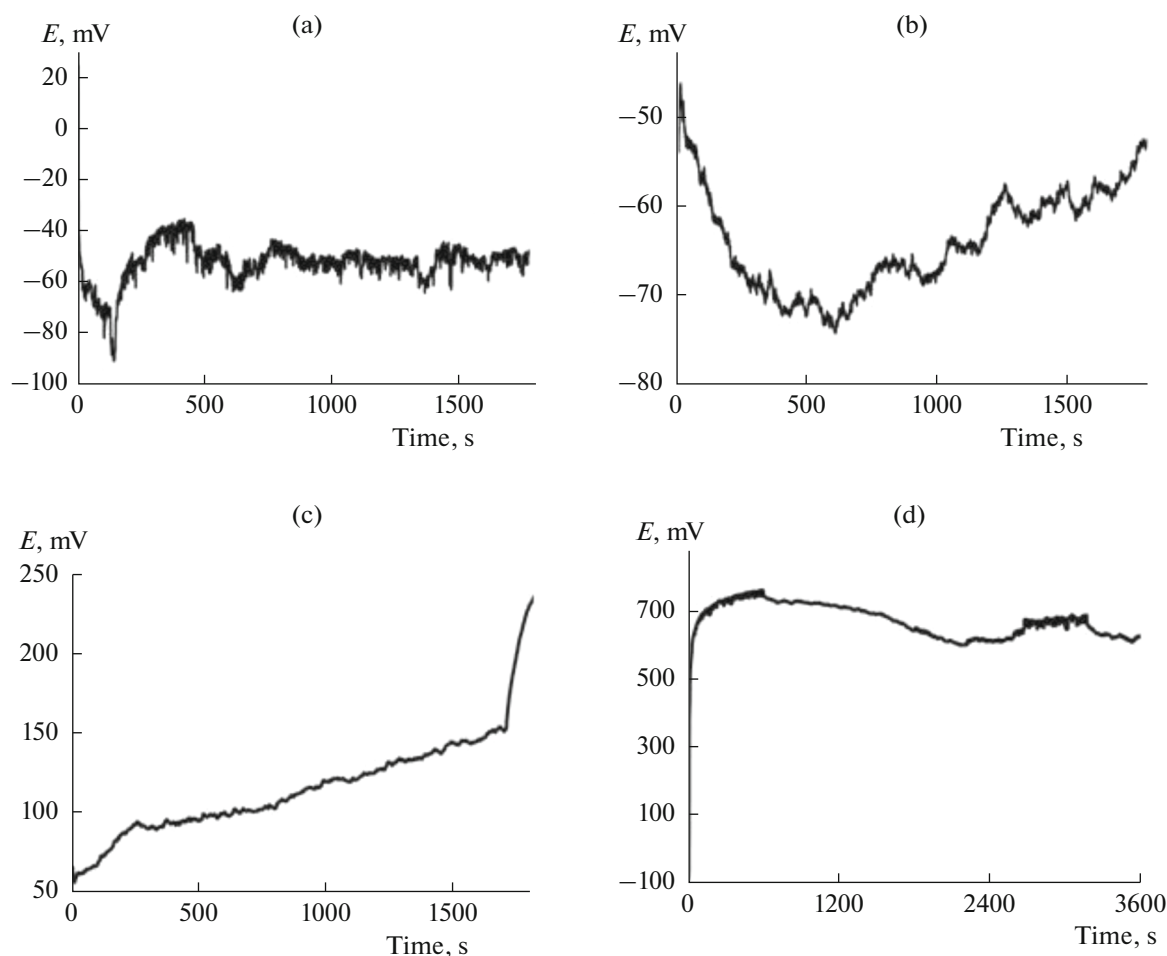


**Fig. 8.** Chronopotentiograms of alloys (a-c)  $Zn_{0.67}Ag_{0.33}$  and (d)  $Zn_{0.46}Ag_{0.54}$  in  $(LiCl)_{0.57}(CsCl)_{0.26}(KCl)_{0.17}$  melt at the current density,  $mA/cm^2$ : (a) 20, (b) 35, (c) 50, (d) 7.

pores of up to  $4\ \mu m$ , which formed joints of  $5\text{--}20\ \mu m$  length with pores between them up to  $10\ \mu m$ . The zinc content in this surface layer approached zero. The morphology of the thus obtained phase of metal silver

considerably differed from the more uniform structure of pores and ligaments obtained at the higher current densities. It resembled more likely a network of branched dendrites but with considerable connectivity.

**Table 2.** Conditions and results of electrochemical dealloying

Alloy	Dealloying potential, V	Current density, $mA/cm^2$	Dealloying time, s	Pore size, $\mu m$	Residual Zn content, mol %
$Zn_{0.67}Ag_{0.33}$	-0.60	20	1800	Rare pores and indentations	63
	-0.55		2430	0.1–1	10
			2340	0.5–2	$\approx 0$
			12600	1–5	10
			1800	0.5–1	10
1800	1–3	20			
$Zn_{0.46}Ag_{0.54}$	-0.18	7	1800	Rare pores and indentations	1–3
			3600	0.1–1 0.5–4; 5–20	$\approx 0$

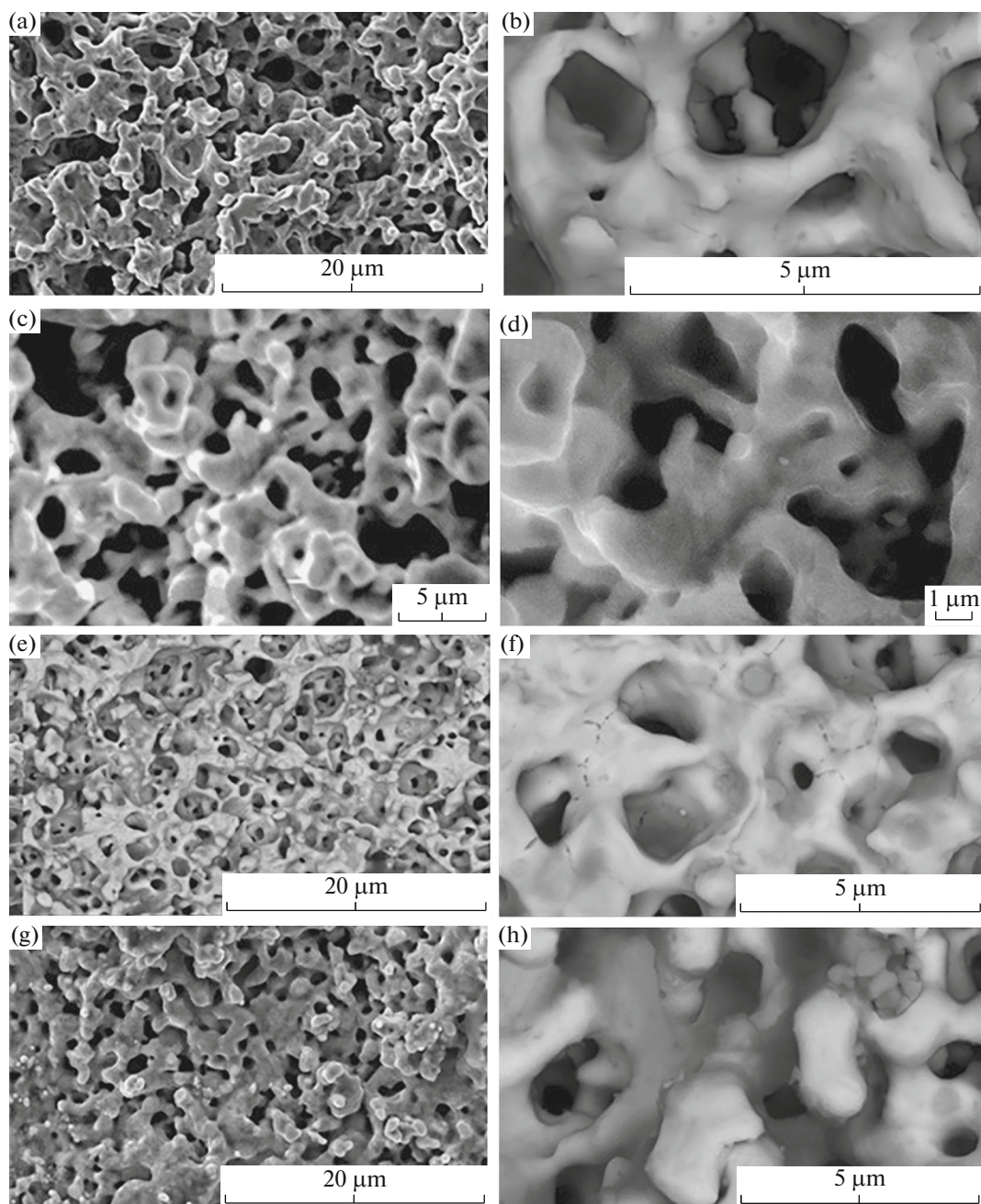


**Fig. 9.** Microimages of the surface of  $Zn_{0.67}Ag_{0.33}$  alloy after dealloying in  $(LiCl)_{0.57}(CsCl)_{0.26}(KCl)_{0.17}$  melt at the current density,  $mA/cm^2$ : (a–d) 20, (e, f) 35, and (g, h) 50. Electrolysis time, s: (a, b) 2300, (c, d) 12600, and (e–h) 1800.

This is why it seems interesting to study certain functional properties of synthesized materials, namely, their mechanical and electrocatalytic properties.

Table 2 summarizes the conditions and results of experiments performed.

## CONCLUSIONS

(1) The possibility of percolation dealloying of single-phase alloys  $Zn_{0.67}Ag_{0.33}$  and  $Zn_{0.46}Ag_{0.54}$  in the

$(LiCl)_{0.57}(CsCl)_{0.26}(KCl)_{0.17}$  eutectics at  $300^{\circ}C$  to form ultraporous metals of various morphology is demonstrated.

(2) It is shown that the virtually complete removal of zinc from the surface is reached by dealloying under galvanostatic conditions at the current density of about 20 for the  $\epsilon$  phase and  $7 mA/cm^2$  for the  $\beta$  phase of the Ag–Zn alloy. The selectivity of alloy dissolution decreases as the current density increases.

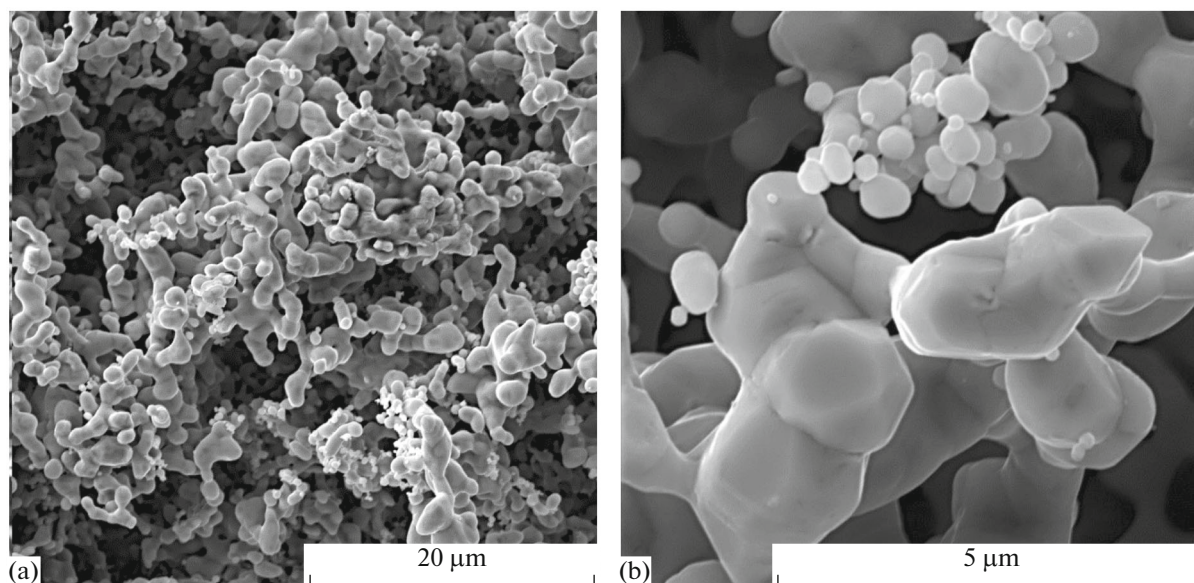


Fig. 10. Microimages of the surface of  $Zn_{0.46}Ag_{0.54}$  alloy after its dealloying by the current density of  $7 \text{ mA/cm}^2$  for 3600 s.

(3) The galvanostatic dealloying of the  $Zn_{0.67}Ag_{0.33}$  alloy leads to formation of characteristic uniform porous structures with pores and ligaments of approximately the same size lying in the interval of  $0.5\text{--}5 \mu\text{m}$ .

(4) The galvanostatic dealloying of the  $Zn_{0.46}Ag_{0.54}$  alloy produces the dendrite structure formed by branched corallites with the characteristic size of agglomerates of about  $0.5\text{--}4$  and  $5\text{--}20 \mu\text{m}$ .

#### ACKNOWLEDGEMENTS

The study was carried out with the use of equipment of the Center of Collective Use “Substance Composition” at the Institute of High Temperature Electrochemistry, Ural Branch, Russian Academy of Sciences. We are grateful to A.A. Pankratova, V.B. Malkova, B.D. Antonova, and N.I. Moskalenko for carrying out the analyses.

#### FUNDING

The study was supported by the Russian Foundation for Basic Research (project no. 20-03-00267a).

#### CONFLICT OF INTEREST

The authors declare that they have no conflict of interest.

#### REFERENCES

- Zhang, J. and Li, Ch.M., Nanoporous metals: fabrication strategies and advanced electrochemical applications in catalysis, sensing and energy systems, *Chem. Soc. Rev.*, 2012, vol. 41, p. 7016.
- Weissmüller, J. and Sieradzki, K., Dealloyed nanoporous materials with interface-controlled behavior, *MRS Bull.*, 2018, vol. 43, p. 14.
- Delgado, J., Benkirane, A., Claver, C., Curulla-Ferre, D., and Godard, C., Advances in the preparation of highly selective nanocatalysts for the semi-hydrogenation of alkynes using colloidal approaches, *Dalton Trans.*, 2017, vol. 46, p. 12381.
- Yang, W., Ma, W., Zhang, Zh., and Zhao, Ch., Ligaments size-dependent electrocatalytic activity of nanoporous Ag network for  $\text{CO}_2$  reduction, *Faraday Discuss.*, 2018, vol. 210, p. 289.
- Li, Zh., Lu, X., Li, B., Lu B., and Wang, Q., Research on electrochemical oxidation of formaldehyde on the nanoporous silver electrode in alkaline solution, *ECS Electrochem. Lett.*, 2015, vol. 4, p. H24.
- Barsuk, D., Zadick, A., Chatenet, M., Georganakis, K., Panagiotopoulos, N., Champion, Y., and Alberto Moreira, J., Nanoporous silver for electrocatalysis application in alkaline fuel cells, *Mater. Des.*, 2016, vol. 111, p. 528.
- Zhang, Y., Luc, W., Hutchings, G.S., and Jiao, F., Photoelectrochemical carbon dioxide reduction using a nanoporous Ag cathode, *ACS Appl. Mater. Interfaces*, 2016, vol. 8, p. 24652.
- Su, L. and Gan, Y.X., Nanoporous Ag–Sn anodes for energy conversion in photochemical fuel cells, *Mater. Des.*, 2016, vol. 111, p. 528.
- Ma, Ch., Trujillo, M.J., and Camden, J.P., Nanoporous silver film fabricated by oxygen plasma: A facile approach for SERS substrates, *ACS Appl. Mater. Interfaces*, 2016, vol. 8, p. 23978.
- Detsi, E., Sánchez Sellès, M., Onck Jeff, Th, p., and Hosson, M.De., Nanoporous silver as electrochemical actuator, *Scr. Mater.*, 2013, vol. 69, p. 195.
- Lizhi, Y., Luhua, J., Tianran, Zh., Guoxiong, W., Suli, W., Xinhe, B., and Gongquan, S., Electrochemically synthesized freestanding 3D nanoporous silver electrode with high electrocatalytic activity, *Catal. Sci. Technol.*, 2016, vol. 6, p. 7163.



12. Marshakov, I.K., Vvedenskii, A.V., Kondrashin, V.Yu., and Bokov, G.A. *Anodnoe rastvorenje i selektivnaya korrozija splavov* (Anodic Dissolution and Selective Corrosion of Alloys), Voronezh: Voronezh. Univ., 1988.
13. Pertsov, N.V., Zozulya, V.V., and Prokopenko, V.A., Formation of a porous material upon electrochemical leaching of a homogeneous gold-containing alloy, *Colloid J.*, 2000, vol. 62, no. 1, p. 119.
14. Li, Zh., Wang, D., Li, B., and Lua, The dealloying kinetics of Ag<sub>25</sub>Zn<sub>75</sub> in 0.1 M H<sub>2</sub>SO<sub>4</sub>, *J. Electrochem. Soc.*, 2010, vol. 157, p. K223.
15. Li, Z.Q., Li, B.Q., Qin, Z. X., and Lu, X., Fabrication of porous Ag by dealloying of Ag–Zn alloys in H<sub>2</sub>SO<sub>4</sub> solution, *J. Mater. Sci.*, 2010, vol. 45, p. 6494.
16. Li, Zh., Lu, X., and Qin, Z., Formation of nanoporous silver by dealloying Ag<sub>22</sub>Zn<sub>78</sub> alloy at low temperature in H<sub>2</sub>SO<sub>4</sub>, *Int. J. Electrochem. Sci.*, 2013, vol. 8, p. 3564.
17. Li, Zh., Bai, L., and Lu, X., Inhomogeneity of bulk nanoporous silver fabricated via dealloying Ag–Zn alloy in sulphuric acid, *Micro Nano Lett.*, 2013, vol. 8, p. 805.
18. Zhang, Ch., Sun, J., Xu, J., Wang, X., Ji, H., Zhao, Ch., and Zhang, Zh., Formation and microstructure of nanoporous silver by dealloying rapidly solidified Zn–Ag alloys, *Electrochim. Acta*, 2012, vol. 63, p. 302.
19. Li, Zh., Wang X., and Lu X., Refinement of nanoporous silver by adding surfactant to the electrolyte, *ECS Electrochem. Lett.*, 2014, vol. 3, p. C13.
20. Zhao, X., Wang, F., Li, R.W., Zhang, J.C., and Huang, M.Wu., Effect of Ag content on phase evolution during the de-alloying of Ag–Al alloy: Combining the electrochemical noise with the wavelet and analysis, *Int. J. Electrochem. Sci.*, 2017, vol. 12, p. 11150.
21. Song, T., Gao Y., Zhang, Zh., and Zhai, Q., Dealloying behavior of rapidly solidified Al–Ag alloys to prepare nanoporous Ag in inorganic and organic acidic media, *Cryst. Eng. Comm.*, 2011, vol. 13, p. 7058.
22. Li, G., Song, X., Lu, F., and Sun, Zh., Formation and control of nanoporous Ag through electrochemical dealloying of the melt-spun Cu–Ag–Ce alloys, *J. Mater. Res.*, 2012, vol. 27, p. 1612.
23. Xu, H. and Zhang, T., Formation of ultrafine spongy nanoporous metals (Ni, Cu, Pd, Ag and Au) by dealloying metallic glasses in acids with capping effect, *Corr. Sci.*, 2019, vol. 153, p. 1.
24. Yeh, F.-H., Tai, Ch.-Ch., Huang, J.-F., and Sun, I.-W., Formation of porous silver by electrochemical alloying/dealloying in a water-insensitive zinc chloride-1-ethyl-3-methyl imidazolium chloride ionic liquid, *J. Phys. Chem. B*, 2006, vol. 110, p. 5215.
25. Sitnikov, L.V., Kulik, N.P., Tkachev, N.K., Pankratov, A.A., Malkov, V.B., Ivenko, V.M., Molchanova, N.G., Moskalenko, N.I., and Antonov, B. D., Selective anodic dissolution of gold alloys in a molten eutectic mixture of cesium, potassium, sodium chlorides, *Rasplavy*, 2018, no. 4, p. 463.
26. Nikitina, E.V., Kazakovtseva, N.A., Tkachev, N.K., Karfidov, E.A., Maikov, M.A., and Malkov, V.B., Selective dissolution of brass in molten eutectic mixture of carbonates of lithium, sodium, potassium, *Rasplavy*, 2017, no. 6, p. 565.
27. HSC 6.12. Outotec Research Oy, 1974–2007.
28. Lyakishev, N.P., *Diagrammy sostoyaniya dvoynykh metallicheskih sistem* (Phase Diagrams of Binary Metal Systems), Moscow: *Mashinostroenie*, 1996, vol. 1, p. 109.
29. Xu, J., Wang, Y., and Zhang, Zh., Potential and concentration dependent electrochemical dealloying of Al<sub>2</sub>Au in sodium chloride solutions, *J. Phys. Chem. C*, 2012, vol. 116, p. 5689.

Translated by T. Safonova